AGU PUBLICATIONS

Radio Science

RESEARCH ARTICLE
10.1002/2017RS006473

Compressive MIMO Beamforming of Data Collected in a Refractive Environment

Mark Wagner[1], **Santosh Nannuru**[1], **and Peter Gerstoft**[1]

[1] Scripps Institution of Oceanography, University of California, San Diego, La Jolla, CA, USA

Key Points:
- Compressive sensing can be used for efficient beamforming of MIMO channels
- Atmospheric refractivity can influence the shape of a MIMO channel
- MIMo channels evolve in tandem with atmospheric refractivity

Correspondence to:
M. Wagner,
m2wagner@eng.ucsd.edu

Citation:
Wagner, M., Nannuru, S., & Gerstoft, P. (2017). Compressive MIMO beamforming of data collected in a refractive environment. *Radio Science*, *52*, 1458–1471. https://doi.org/10.1002/2017RS006473

Received 13 OCT 2017
Accepted 27 OCT 2017
Accepted article online 9 NOV 2017
Published online 4 DEC 2017

Abstract The phenomenon of ducting is caused by abnormal atmospheric refractivity patterns and is known to allow electromagnetic waves to propagate over the horizon with unusually low propagation loss. It is unknown what effect ducting has on multiple input multiple output (MIMO) channels, particularly its effect on multipath propagation in MIMO channels. A high-accuracy angle-of-arrival and angle-of-departure estimation technique for MIMO communications, which we will refer to as compressive MIMO beamforming, was tested on simulated data then applied to experimental data taken from an over the horizon MIMO test bed located in a known ducting hot spot in Southern California. The multipath channel was estimated from the receiver data recorded over a period of 18 days, and an analysis was performed on the recorded data. The goal is to observe the evolution of the MIMO multipath channel as atmospheric ducts form and dissipate to gain some understanding of the behavior of channels in a refractive environment. This work is motivated by the idea that some multipath characteristics of MIMO channels within atmospheric ducts could yield important information about the duct.

Plain Language Summary Long-range ship to ship wireless communication is difficult because the horizon can obstruct the line of sight path between ships, causing radio signal strength to decrease rapidly with range. Sometimes, however, an event known as ducting can occur which allows radio waves to curve over the horizon. Multiple input multiple output (MIMO) radio setups can exploit knowledge of the paths taken by the signal from transmitter to receiver to increase communication strength. In this paper we take measurements from a MIMO radio setup located in a region known for ducting and observe the evolution of the signal paths, looking for patterns that may be used to predict properties of atmospheric ducts.

1. Introduction

For long-range wireless electromagnetic (EM) communication signals, the line of sight path between transmitter and receiver can be obscured by the curvature of the Earth. Generally, signal strength at the receiver fades quickly with range for over the horizon signals, but an exception can be made for marine environments experiencing atmospheric ducting (Haack & Burk, 2001). Ducting causes trapping of EM waves propagating at low angles between the ocean's surface and the top of the duct (Craig & Levy, 1991). Ducts are formed by certain atmospheric refractivity profiles, where refractivity is a measure of the deviation of an electromagnetic wave from a straight line path due to variation in air density as a function of height. In a ducting environment an EM wave can be guided over the horizon through a path that it would not otherwise travel (Wagner et al., 2016). This effect is known to decrease signal attenuation over long ranges but may also cause multipath interference in the form of multipath fading (Timmins & O'Young, 2009).

In a ducting environment it is hypothesized that communication channels may have higher throughput (Gerstoft et al., 2003) and may also take on unique properties based on the duct. To test this hypothesis, an experimental test bed was set up where a 4×4 multiple input multiple output (MIMO) communications array was placed on vertical masts 41 km apart in a ducting hot spot in Southern California (Haack & Burk, 2001); see Figure 1. Pilot signals from the transmitters were recorded by the receivers at regular intervals for 18 days. The goal of the experiment was to observe the change in the multipath environment for an over the horizon channel during ducting events. Ducting events were identified by significant increases in received power levels at the receiver array.

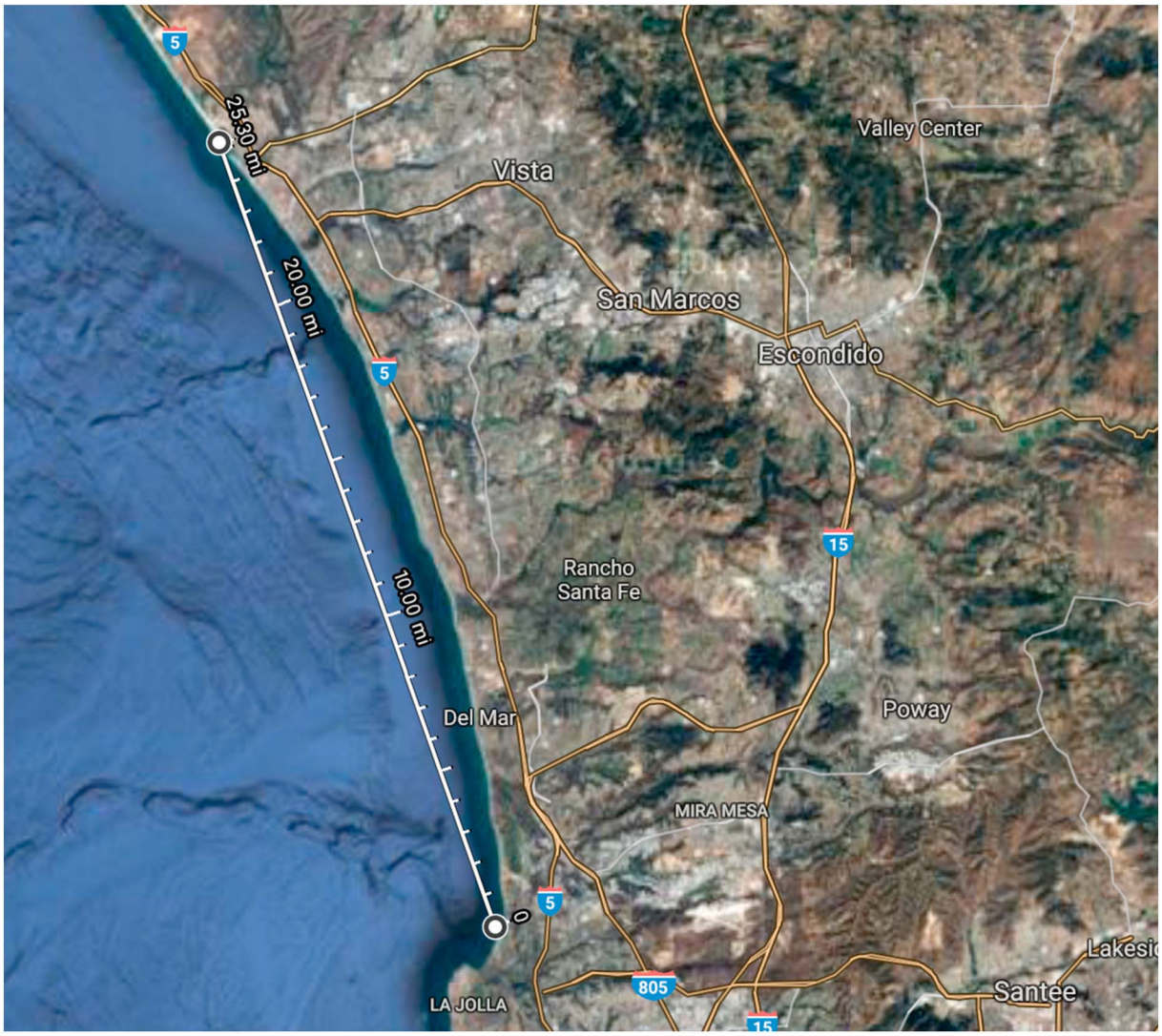

Figure 1. Shortest path between transmitter (bottom) and receiver (top) superimposed on satellite image of Southern California.

We are unaware of any other experiment to date having been performed for the purpose of relating the multipath characteristics of a MIMO channel to atmospheric refractivity. While the over the horizon MIMO channel data that was collected is unique, it is also limited in that it is representative of one static channel which may not be representative of all ducting channels. Our hope is that a better understanding of the impact of ducting on MIMO communications channels will lead to more effective refractivity estimation techniques. For instance, if the multipath channel takes on specific properties exclusively during ducting events, this information could be used to more accurately identify the presence and properties of a duct.

In this paper we use compressive MIMO beamforming to determine the angle of arrival (AoA) and angle of departure (AoD) of signals traveling through a channel. Compressive MIMO beamforming (detailed in section 3.2) is a precision beamforming technique utilizing compressed sensing and is based on the assumption of signal sparsity (Mecklenbrauker et al., 2017; Tse & Viswanath, 2005) in the transmit and receive angle domain. To obtain a best estimate of the MIMO channel matrix (see section 2; Biguesh & Gershman, 2006; Wang et al., 2007), a set of optimal training sequences (Chu, 1972) (see section 5) were sent from the transmitter array. From the channel matrix a virtual array (Wang, 2012) is formed, to which compressive MIMO beamforming can be applied to obtain the transmit and receive angles of the signal.

The structure of the paper is as follows. In section 2 the signal model is explained and theoretical framework for channel estimation is laid out. Optimal channel estimation is essential to this work because knowledge

of the MIMO channel is required for beamforming. Section 3 gives the theory behind compressive sensing and lays the framework for MIMO beamforming. Section 4 gives compressive MIMO beamforming error rates in two metrics for simulated signals of varying signal-to-noise ratio (SNR) and number of active signal paths. Section 5 describes the experimental test bed and details regarding the transmitted waveforms and their detections. Experimental data are processed, and the resulting multipath channels and channel properties are analyzed in section 6.

2. Multipath Signal Model

2.1. MIMO Signal Model

MIMO systems are a well-studied topic in antenna communications and offer several benefits over single input and output systems. A MIMO system is defined as an antenna setup utilizing multiple transmitters and receivers, often positioned in an array. By increasing the number of transmitters and receivers the dimension of the channel matrix, whose elements represent the transfer function between each transmitter and receiver, is increased. Higher-dimensional channel matrices can be exploited by spatially multiplexing multiple streams of information (Bolcskei et al., 2002). Having multiple receivers allows for spatial processing (more generally known as beamforming) to estimate the receive angle of arriving signals, while multiple transmitters allow for spatial processing for estimation of the transmit angle of arriving signals.

The position of transmitters and receivers in a MIMO system is flexible, though this paper will focus on transmit and receive elements positioned in uniform linear arrays (ULAs). Consider N_T transmitters and N_R receivers with element spacing r and s, communicating over a single frequency. The set of transmitters send signals $\mathbf{x}_t \in \mathbb{C}^{N_T}$ at time sample time $t = 1 \dots T$. Each of P paths has a unique AoD ϕ_p, AoA θ_p, and corresponding complex path gain.

Assuming a time invariant channel, the received signal at time sample t, $\mathbf{y}_t \in \mathbb{C}^{N_R}$ is

$$\mathbf{y}_t = \mathbf{H}\mathbf{x}_t + \mathbf{w}_t, \tag{1}$$

where $\mathbf{w}_t \in \mathbb{C}^{N_R}$ is a zero mean symmetric complex Gaussian noise vector at time t and $\mathbf{H} \in \mathbb{C}^{N_R \times N_T}$ is the channel matrix which can be further decomposed (Tse & Viswanath, 2005)

$$\mathbf{H} = \sum_{p=1}^{P} a_p \mathbf{a}_R(\theta_p)\mathbf{a}_T(\phi_p)^H, \tag{2}$$

where a_p is the complex gain of path p, $\mathbf{a}_R(\theta) \in \mathbb{C}^{N_R}$, and $\mathbf{a}_T(\phi) \in \mathbb{C}^{N_T}$ are the receive and transmit steering vectors for angles θ and ϕ, whose ith element is defined as $\mathbf{a}_{T,i}(\theta) = \exp[-j2\pi r \sin(\theta) i/\lambda]$ for $i = [0, \dots, N_T - 1]$ and $\mathbf{a}_{R,i}(\theta) = \exp[-j2\pi s \sin(\theta) i/\lambda]$ for $i = [0, \dots, N_R - 1]$ with $j = \sqrt{-1}$, s and r are transmitter and receiver array spacings in meters, and λ is the carrier wavelength in meters (Pesavento et al., 2004). Equation (2) implicitly assumes that the received signals arrive as plane waves at the receiver.

The channel described by equations (1) and (2) can be equivalently viewed as the sum of channels from every possible signal path. Rather than express the channel in (2) as the sum of array responses from each of P paths, it can also be expressed as the sum of array responses from every possible path over the space of possible transmit and receive angles (θ, ϕ), only a few of which will be active (take nonzero values). Formally,

$$\mathbf{H} = \int_{\phi} \int_{\theta} \mathbf{H}^a(\theta, \phi)\mathbf{a}_R(\theta)\mathbf{a}_T(\phi)^H \, \mathrm{d}\theta \, \mathrm{d}\phi, \tag{3}$$

where $\mathbf{H}^a(\theta, \phi)$ is a function representing the path gain from transmit and receive angles θ and ϕ. Since we have made the assumption that $\mathbf{H}^a(\theta, \phi)$ is nonzero at only a few points, an approximate discretization can be made

$$\mathbf{H} \approx \sum_{i}^{Q_R} \sum_{j}^{Q_T} \mathbf{H}^a_{i,j} \mathbf{a}_R(\theta_i)\mathbf{a}_T^H(\phi_j), \tag{4}$$

where Q_R and Q_T are the number of points to which the transmit and receive angle space are quantized. The approximation of equation (4) replaces the continuous function $\mathbf{H}^a(\theta, \phi)$ with sparse matrix $\mathbf{H}^a \in \mathbb{C}^{Q_R \times Q_T}$,

(having exactly P nonzero entries) which we will refer to as the angular domain channel matrix (Chan et al., 2008). Plugging (4) into (1), we have

$$\mathbf{y}_t \approx \sum_{i}^{Q_R} \sum_{j}^{Q_T} \mathbf{H}^a_{i,j} \mathbf{a}_R(\theta_i) \mathbf{a}_T^H(\phi_j) \mathbf{x}_t + \mathbf{w}_t, \tag{5}$$

which is an alternative signal model utilizing sparsity. The focus of this paper is the estimation of $\mathbf{H}^a$. From known $\mathbf{x}_t$ and measurements of $\mathbf{y}_t$ we estimate $\mathbf{H}$, then using sparse processing detailed in section 3, an estimate of $\mathbf{H}^a$ is constructed from $\mathbf{H}$. Once recovered, we analyze the transmit and receive angles traveled by multipath signals propagating through ducting environments to determine any special properties they may have which could be used to characterize ducts.

The elements of the steering vectors $\mathbf{a}_R(\theta)$ and $\mathbf{a}_T(\phi)$ are unit magnitude complex values representing the relative phase shift of the signals arriving or departing from one antenna with respect to a reference antenna. From their definitions, the phase shift between vector elements is dependent on carrier signal wavelength, arrival/departure angle, and interelement array spacing. Ideally, inter element spacing should be one half the carrier signal wavelength, which results in maximum angular resolution of $\pm 90°$ and is known as critical spacing. Sparsely spaced array elements result in angle ambiguities caused by aliasing, while densely spaced arrays have smaller array aperture leading to lower angular resolution. For sparsely spaced arrays, $\theta_{\max} = \sin^{-1}(\frac{\lambda}{2r})$ where $\theta_{\max}$ is the maximum resolvable receive angle, r is the inter element spacing, and λ is the wavelength of the carrier signal in meters.

2.2. Channel Estimation

Compressive MIMO beamforming takes the estimated channel matrix $\mathbf{H}$ as input. The estimate, $\hat{\mathbf{H}}$ (where $\hat{}$ indicates an estimate), must be made from the known transmitted and measured received signals. In this section we derive criteria for the transmitted waveform such that the resulting channel estimate is optimal. Later in section 5 the waveform transmitted from the experimental test bed is described and can be shown to satisfy the criteria for optimal channel estimation.

Consider a matrix $\mathbf{X} \in \mathbb{C}^{N_T \times T}$ whose columns $\mathbf{x}_t$ represent the symbols sent from all transmitters at time $t = [1, \ldots, T]$ and matrix $\mathbf{Y} \in \mathbb{C}^{N_R \times T}$ whose columns $\mathbf{y}_t$ contain the received symbols at time $t = [1, \ldots, T]$. $\mathbf{Y}$ can be expressed as

$$\mathbf{Y} = \mathbf{H}\mathbf{X} + \mathbf{W}, \tag{6}$$

where $\mathbf{W} \in \mathbb{C}^{N_R \times T}$ is complex Gaussian sensor noise distributed such that each column $\mathbf{w}_t \sim \mathcal{CN}(\mathbf{0}, \sigma^2 \mathbf{I}_T)$ for $t = [1, \ldots, T]$, where $\mathbf{I}_T$ is the identity matrix of dimension T. In this case the least squares channel estimator is (Biguesh & Gershman, 2006)

$$\hat{\mathbf{H}} = \mathbf{Y}\mathbf{X}^{\dagger}, \tag{7}$$

where $\mathbf{X}^{\dagger} = \mathbf{X}^H(\mathbf{X}\mathbf{X}^H)^{-1}$ is the pseudoinverse. Training matrix $\mathbf{X}$ is constrained by the transmitted power as

$$\|\mathbf{X}\|_F^2 = \mathrm{tr}(\mathbf{X}\mathbf{X}^H) = \mathcal{P}, \tag{8}$$

where tr[.] is the trace operation and $\mathcal{P}$ is a known constant representing the total power transmitted and $\|.\|_F$ is the Frobenius norm. We wish to find a training matrix $\mathbf{X}$ which minimizes the channel estimation error subject to the power constraint (8). This is equivalent to solving the optimization problem

$$\min_{\mathbf{X}} \mathrm{E}\left[\|\mathbf{H} - \hat{\mathbf{H}}\|_F^2\right] \qquad \text{s.t.} \quad \mathrm{tr}(\mathbf{X}\mathbf{X}^H) = \mathcal{P}, \tag{9}$$

where E[.] is the expected value. Combining (6) and (7), we see $\mathbf{H} - \hat{\mathbf{H}} = \mathbf{W}\mathbf{X}^{\dagger}$. Continuing from (9), we get the objective function

$$\begin{aligned} J &= \mathrm{E}\left[\|\mathbf{H} - \hat{\mathbf{H}}\|_F^2\right] \\ &= \mathrm{E}\left[\|\mathbf{W}\mathbf{X}^{\dagger}\|_F^2\right] \\ &= \sigma_n^2 N_R \mathrm{tr}\left[\mathbf{X}^{\dagger H}\mathbf{X}^{\dagger}\right] \\ &= \sigma_n^2 N_R \mathrm{tr}\left[(\mathbf{X}\mathbf{X}^H)^{-1}\right], \end{aligned} \tag{10}$$

where $\mathrm{E}[\mathbf{W}^H\mathbf{W}] = \sigma_n^2 N_R \mathbf{I}$. Plugging (10) into (9), an equivalent equation is

$$\min_{\mathbf{X}} \mathrm{tr}\left[(\mathbf{X}\mathbf{X}^H)^{-1}\right] \quad \text{s.t.} \quad \mathrm{tr}\left[\mathbf{X}\mathbf{X}^{\mathrm{H}}\right] = \mathcal{P}. \tag{11}$$

From here any training matrix satisfying

$$\mathbf{X}\mathbf{X}^H = \frac{\mathcal{P}}{N_T}\mathbf{I} \tag{12}$$

is optimal for (11) (Biguesh & Gershman, 2006). The optimality criteria also simplify the channel estimation equation. Plugging (12) into (7), we have

$$\hat{\mathbf{H}} = \left(\frac{N_T}{\mathcal{P}}\right)\mathbf{Y}\mathbf{X}^H. \tag{13}$$

All matrices with orthogonal rows with the same norm satisfy the optimality criteria of equation (12). The waveforms transmitted by the MIMO test bed described in section 5 satisfy (12).

3. Compressive MIMO Beamforming

3.1. Review of Compressive Sensing

Compressive sensing (CS) is a relatively new field of signal processing wherein a measurement vector is reconstructed as a sparse linear combination of predetermined dictionary vectors. Consider the classical linear measurement model

$$\mathbf{r} = \mathbf{\Psi}\mathbf{t} + \mathbf{w}, \tag{14}$$

where $\mathbf{w}$ is Gaussian noise and $\mathbf{r}$ is a known measurement composed of some linear combination of the columns of known dictionary matrix $\mathbf{\Psi}$. The goal of CS is to reliably determine $\mathbf{t}$ from knowledge of $\mathbf{r}$ and $\mathbf{\Psi}$ given that $\mathbf{t}$ is sparse (has few nonzero values) or approximately sparse (has entries that decay rapidly when reordered by magnitude).

The central tenet of CS is that if $\mathbf{t}$ is sparse then most of the salient information in $\mathbf{r}$ can be captured by a few dictionary vectors (for appropriately designed dictionaries). Additionally, recent theoretical results have established that $\mathbf{t}$ can be solved using tractable mixed norm optimization programs (Chen et al., 2001; Tibshirani, 1996), efficient greedy algorithms (Mallat & Zhang, 1993), fast iterative thresholding algorithms (Daubechies et al., 2004), or Bayesian probabilistic methods (Tipping, 2001). Proofs establishing the reliability of the mentioned reconstruction procedures depend on a certain property of the dictionary matrix $\mathbf{\Psi}$ and the sparsity of $\mathbf{t}$. Specifically, the key property of $\mathbf{\Psi}$ for proving the optimality of reconstruction is the restricted isometry property (RIP) (Candes, 2008).

There are currently no known algorithms that check the RIP for a given matrix in polynomial time, though one of the reasons that has lead to the widespread use of CS in many fields is the discovery that certain probabilistic constructions of matrices satisfy the RIP with high probability (Rudelson & Vershynin, 2008). In this paper we assume that the RIP holds for the dictionary matrix defined in section 3.2 and test this theory with simulations performed in section 4.

Of the many CS reconstruction algorithms noted earlier, we use the LASSO (Tibshirani, 1996) (which is sometimes also referred to as basis pursuit denoising (Chen et al., 2001)). The LASSO is a well-studied method for solving compressive sensing problems which has good reconstruction error bounds (Bickel et al., 2009) and is computationally attractive due to the many publicly available software packages for computing it. The LASSO in Lagrangian form is

$$\min_{\mathbf{t}} \|\mathbf{r} - \mathbf{\Psi}\mathbf{t}\|_2^2 + \mu\|\mathbf{t}\|_1, \tag{15}$$

where μ is a positive regularization parameter satisfying $0 \leq \mu \leq 2\|\mathbf{\Psi}^H\mathbf{r}\|_\infty$ (Mecklenbrauker et al., 2017). In the next section we will show that the path angles traveled by a multipath MIMO signal can be solved using the LASSO.

3.2. MIMO Beamforming

From section 2.2 it is clear that an estimate of a channel $\mathbf{H}$ can be made from MIMO systems transmitting certain sequences. Additionally, from equation (2) we see that a MIMO channel can be written as the sum of a small number of paths; thus, the channel is sparse in the dictionary formed from the array responses from each possible path angle. In general, we will only have estimates of the channel, $\hat{\mathbf{H}}$ (from equation (13), which are used to produce angular domain channel estimates, $\hat{\mathbf{H}}^a$.

Define $\mathbf{h} = \text{vec}(\mathbf{H})$ where vec (.) stacks the columns of a matrix and $\tilde{\mathbf{a}}(\theta_p, \phi_p) = \mathbf{a}_R(\theta_p) \otimes \mathbf{a}_T(\phi_p)$ where $\otimes$ is the Khatri-Rao product (Steffens et al., 2016). The dictionary $\mathbf{A}_D \in \mathbb{C}^{Q_R Q_T \times N_R N_T}$ of path angles is defined as

$$\mathbf{A}_D = \left[\tilde{\mathbf{a}}(\theta_1, \phi_1), \ldots, \tilde{\mathbf{a}}(\theta_{Q_R}, \phi_{Q_T})\right], \tag{16}$$

where Q_T and Q_R represent an arbitrary number of transmit and receive angles evenly spaced between $(\phi_{\min}, \phi_{\max})$ and $(\theta_{\min}, \theta_{\max})$. In practical terms, Q_T and Q_R are the number of grid points which the transmit and receive angle space will be divided into. For unknown sparse vector $\mathbf{h}^a = \text{vec}(\mathbf{H}^a) \in \mathbb{C}^{Q_R Q_T}$,

$$\hat{\mathbf{h}} = \mathbf{A}_D \mathbf{h}^a + \boldsymbol{\eta}, \tag{17}$$

where $\boldsymbol{\eta} \in \mathbb{C}^{N_R N_T}$ is the noise due to approximation which is assumed to be from a Gaussian distribution.

Solving equation (15) with variables from equation (17), the LASSO objective function (Donoho, 2006) produces a sparse estimate of the angular domain channel matrix in vector form.

$$\hat{\mathbf{h}}^a = \min_{\mathbf{h}^a} \|\hat{\mathbf{h}} - \mathbf{A}_D \mathbf{h}^a\|_2^2 + \mu \|\mathbf{h}^a\|_1. \tag{18}$$

In this paper we set μ to half its maximum value (see (Mecklenbrauker et al., 2017) for further discussion).

Once $\hat{\mathbf{h}}^a$ has been solved, it is cast back into matrix form, $\hat{\mathbf{H}}^a = \text{vec}^{-1}(\hat{\mathbf{h}}^a)$ which was introduced in equation (4). Each element of the angular domain channel matrix is associated with an AoD and AoA through which the signal could have traveled. The magnitude of each element of $\mathbf{H}^a$ represents the path gain of the signal traveling through the path angle pair associated with that element.

4. Simulation

Compressive MIMO beamforming was simulated and tested against two other beamforming techniques; conventional beamforming (CBF) (Bartlett, 1948) and 2-D MUSIC (Schmidt, 1986), both described in Appendix A. CBF and MUSIC provide estimates of the angular domain power spectrum, which are compared to the estimate produced from compressive MIMO beamforming.

A simulated signal $\mathbf{y}_t \in \mathbb{C}^{N_R}$ was constructed according to equation (5), repeated here for convenience

$$\mathbf{y}_t = \sum_{j=1}^{Q_R} \sum_{i=1}^{Q_T} \mathbf{H}^a_{i,j} \mathbf{a}_R(\theta_j) \mathbf{a}_T^H(\phi_i) \mathbf{x}_t + \mathbf{w}_t = \tilde{\mathbf{y}}_t + \mathbf{w}_t, \tag{19}$$

where $t = [1, \ldots, T]$, $Q_T = Q_R = 30$ and $\mathbf{H}^a$ is a randomly generated sparse matrix whose nonzero elements are unit magnitude with phase drawn from a uniform distribution over the range $[0, 2\pi]$. The sparsity of $\mathbf{H}^a$ was controlled by parameter P ($P = 3$ in Figure 2), and each $\mathbf{x}_t$ was a known realization from a complex normal distribution $\mathbf{x}_t \in \mathbb{C}^{N_T} \sim \mathcal{CN}(\mathbf{0}, \mathbf{I})$ (Gaussian sequences obey equation (12) with high probability) which was generated independently for each t. $\mathbf{y}_t$ was first generated from random but known realizations of $\mathbf{H}^a$ and $\mathbf{x}_t$ then complex Gaussian noise $\mathbf{w}_t \in \mathbb{C}^{N_R} \sim \mathcal{CN}(\mathbf{0}, \boldsymbol{\sigma}^2 \mathbf{I})$ was added such that any desired SNR could be met, where

$$\text{SNR(dB)} = 10 \log \left(\frac{\|\mathbf{H}\mathbf{x}_t\|_2^2}{\|\mathbf{w}_t\|_2^2} \right) = 10 \log \left(\frac{\|\tilde{\mathbf{y}}_t\|_2^2}{\|\mathbf{w}_t\|_2^2} \right). \tag{20}$$

And $\|.\|_2^2$ is the squared ℓ_2 norm.

From $\mathbf{y}_t$ and $\mathbf{x}_t$, $\hat{\mathbf{H}}$ was estimated according to equation (13) with $\mathcal{P} = N_T T$. Given $\hat{\mathbf{H}}$, equation (18) was used to solve for $\hat{\mathbf{H}}^a$. Figure 2 shows plots of $|\mathbf{H}^a|^2$ alongside the angular power spectrum recovered from CBF, ($|\mathbf{H}^a_{\text{CBF}}|^2$ specified in equation (A3) of Appendix A) and MUSIC ($F(\theta, \phi)$ from equation (A6) in Appendix A) applied to the simulated noiseless data with $N_T = N_R = 16$ and $N_T = N_R = 4$.

Note that both CBF and MUSIC are limited by the maximum rank of $\mathbf{H}$, which results in the blurred spectrum seen in Figure 2. The maximum rank of $\mathbf{H}$ is determined by the number of transmitters and receivers in the MIMO system rank $(\mathbf{H}^a) \leq \min(N_T, N_R)$. Compressive MIMO beamforming is not limited in precision by the rank of $\mathbf{H}$ but rather by how many columns of dictionary $\mathbf{A}_D$ can be formed before the dictionary ceases to satisfy the RIP property. When $\mathbf{A}_D$ is populated by too many column vectors $\tilde{\mathbf{a}}(\theta, \phi)$ (which is equivalent to quantizing (θ, ϕ) space too finely), there will be high coherence between the columns of $\mathbf{A}_D$ to the point where the dictionary will cease to satisfy the RIP. It is infeasible to check that any given $\mathbf{A}_D$ satisfies the RIP because

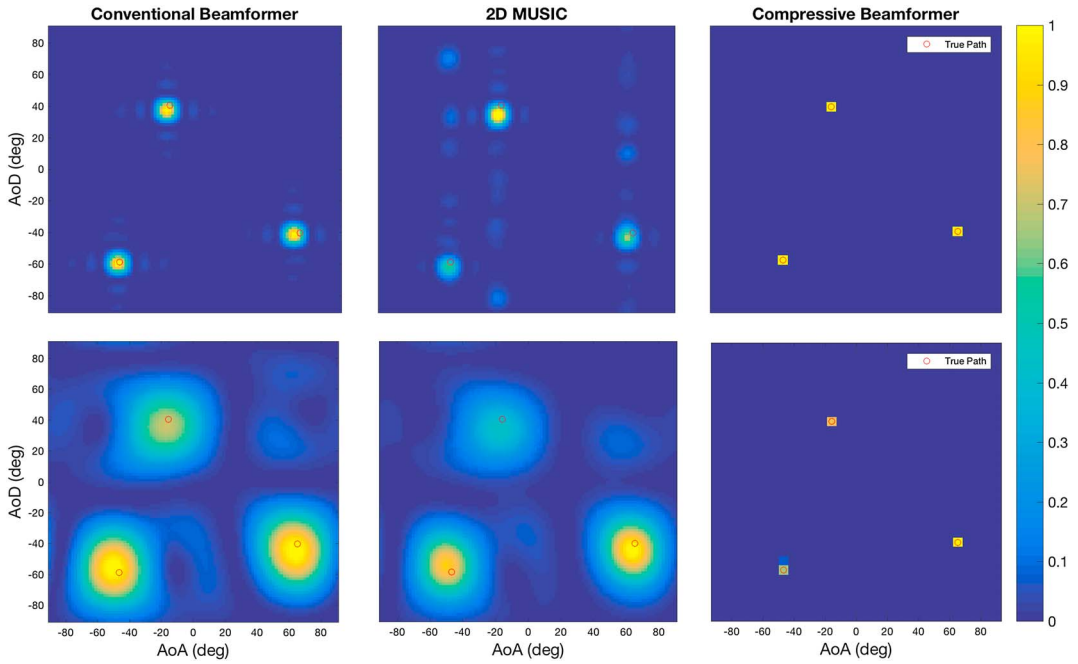

Figure 2. Angular power spectrum from various beamforming techniques performed on simulated noiseless signals with $T = 1,000$,P=3, $\mu = 0.5\mu_{\max}$. (top row) $N_T = N_R = 16$. (bottom row) $N_T = N_R = 4$. (left column) Conventional beamforming, (middle column) 2-D MUSIC, (right column) compressive MIMO beamforming with $Q_R = Q_T = 30$. Transmitter and receiver spacing each set to $\frac{\lambda}{2}$.

there is no known algorithm that works in polynomial time; however, we assume that a dictionary formed from quantizing the angle space into $Q_R = Q_T = 30$ is acceptable because the simulation recovers simulated paths with satisfactory accuracy.

The performance of compressive MIMO beamforming is tested using two error metrics for channels of varying sparsity and SNR given $Q_R = Q_T = 30$. The first error metric, ϵ_A, represents angle error and is defined as the euclidean distance (in (θ, ϕ) space) between the P true path angle pairs of $\mathbf{H}^a$ and the best matching set of P path angle pairs from $\hat{\mathbf{H}}^a$.

$$\epsilon_A = \frac{1}{P}\sum_{p=1}^{P}\sqrt{\left(\hat{\theta}_p - \theta_p\right)^2 + \left(\hat{\phi}_p - \phi_p\right)^2}, \tag{21}$$

where θ_p and ϕ_p are the receive and transmit angles from path p of $\mathbf{H}^a$, $\hat{\theta}_p$ and $\hat{\phi}_p$ are the receive and transmit angles from path p of $\hat{\mathbf{H}}^a$, and the units of ϵ_A are in degrees. The best set of matching paths from $\hat{\mathbf{H}}^a$ was found as the set of paths producing the smallest ϵ_A using exhaustive search. It was found that the number of nonzero elements in $\hat{\mathbf{H}}^a$ was always equal to or greater than that of $\mathbf{H}^a$. Note that simulations were performed over an angle space ranging [−90°, 90°], so an average error of 18° represents a 10% error over the full space. In section 6 we will present findings over a much smaller angle space, for which we expect the same percentage error rather than absolute error.

The second error metric, ϵ_N, isnormed error defined as $\epsilon_N = \frac{1}{P}\|\mathbf{H}^a - \hat{\mathbf{H}}^a\|_F^2$. Normed error is simply a measure of the mean squared difference between the true and estimated angular domain channel matrices.

Each error metric was calculated for $N = 200$ Monte Carlo trials of simulated signals of varying SNR and sparsity then plotted in Figure 3. The random number generator seed was reset for each unique parameterization. We observe that both metrics show positive correlation between error and SNR. Angle error ϵ_A appears nearly constant for signals composed of $P > 1$, indicating that more paths do not lower the angular accuracy of the estimated paths. Normed error curves indicate that the mismatch between true and reconstructed angular channel matrices is much greater for signals from multiple paths. Each curve appears to flatten for SNR above −15 dB. We conclude that compressive MIMO beamforming will have sufficient accuracy for received signals whose SNR is above −15 dB.

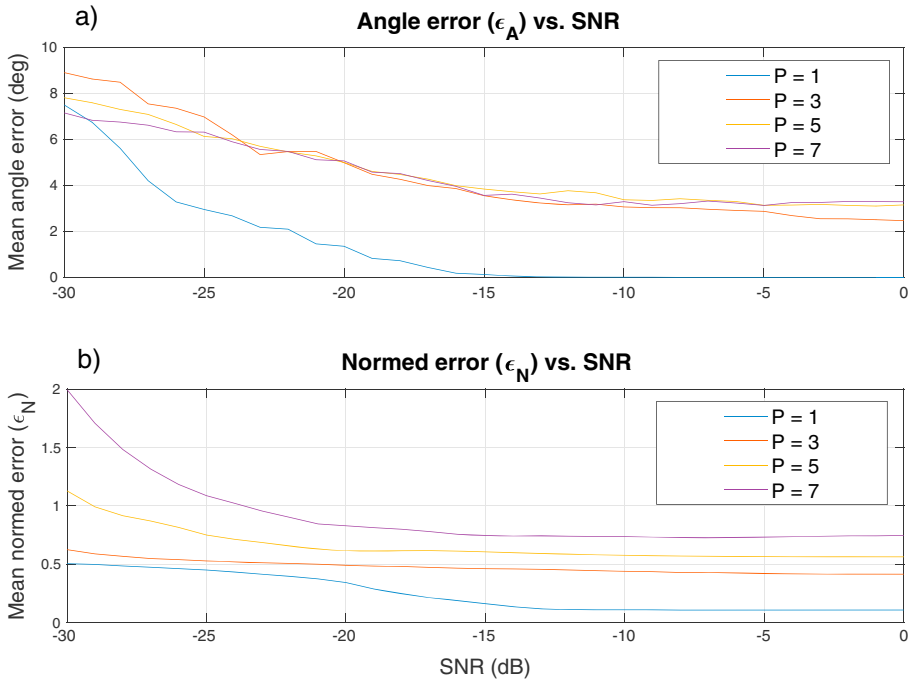

Figure 3. Average error of $N = 200$ Monte Carlo reconstructions of $\hat{\mathbf{H}}^a$ using compressive MIMO beamforming with $\mu = 0.5\mu_{\max}$ on simulated signals of varying SNR and sparsity P. (a) Angle error (ϵ_A). (b) Normed error (ϵ_N).

5. Experimental Setup and Data

The coast of Southern California is known as a hot spot for atmospheric ducts (Haack & Burk, 2001), which can act as leaky waveguides for EM waves. The goal of the experiment was to observe the impact of a ducting environment on a MIMO communications channel, particularly the change in multipath properties of the channel with time. No measurements of the atmospheric refractivity profile were taken, so the observations at the receiver array are understood to reflect the typical characteristics of a refractive channel rather than being the result of any specific type of duct.

5.1. Transmitters and Receivers

Data were collected from vertically positioned ULAs of four transmitters and four receivers. The transmitter array was positioned at the end of Scripps Pier, 332 m from shore, with array spacing of 3.8 m, while the receiver array was located 1,000 m inland at Camp Pendleton with array spacing of 4 m. The transmitters will be referred to as T1 – T4, where T1 is the topmost transmitter. Likewise, the receivers will be referred to as R1 – R4 where R1 is the topmost receiver. From the array spacing the maximum resolvable angles were $\phi_{\max} = 1.63°$ and $\theta_{\max} = 1.55°$, which is within the normal range of expected AoA and AoDs for such long range over the horizon setups (Gerstoft et al., 2003). The topmost elements of the transmitter and receiver arrays were approximately 34 and 32 m above sea level, respectively. The arrays were located 40.72 km apart, far enough that the line of sight path between all antennas was obstructed by the horizon. The elements of both arrays were pointed facing each other in azimuth and with an elevation angle of 0°.

A known, narrowband, length 2^{13} Zadoff-Chu (ZC) signal, $\mathbf{z}$, (Chu, 1972) was sent from each transmitter on carrier frequency 1.385 GHz. ZC signals are complex, constant magnitude, and satisfy the following property

$$\mathbf{z}^H(\mathbf{P}\mathbf{z}) = 0, \tag{22}$$

where $\mathbf{P}$ is any cyclic permutation of the identity matrix with $\mathbf{P} \neq \mathbf{I}$. Equation (22) should be interpreted to mean that any ZC sequence is orthogonal to any circularly shifted version of itself. By sending identical ZC signals with unique circular shifts from each transmitter, a training matrix which satisfies (12) is formed. The transmitted waveforms from [T1, … ,T4] were identical, circularly shifted ZC sequences, $\mathbf{X} \in \mathbb{C}^{N_T \times 2^{13}} = [\mathbf{z}_0, \mathbf{z}_{500}, \mathbf{z}_{1200}, \mathbf{z}_{2000}]^T$ where $\mathbf{z}_i$ is a ZC sequence circularly shifted by i samples. Each snapshot is $8 \times 2^{13} = 2^{16}$ samples.

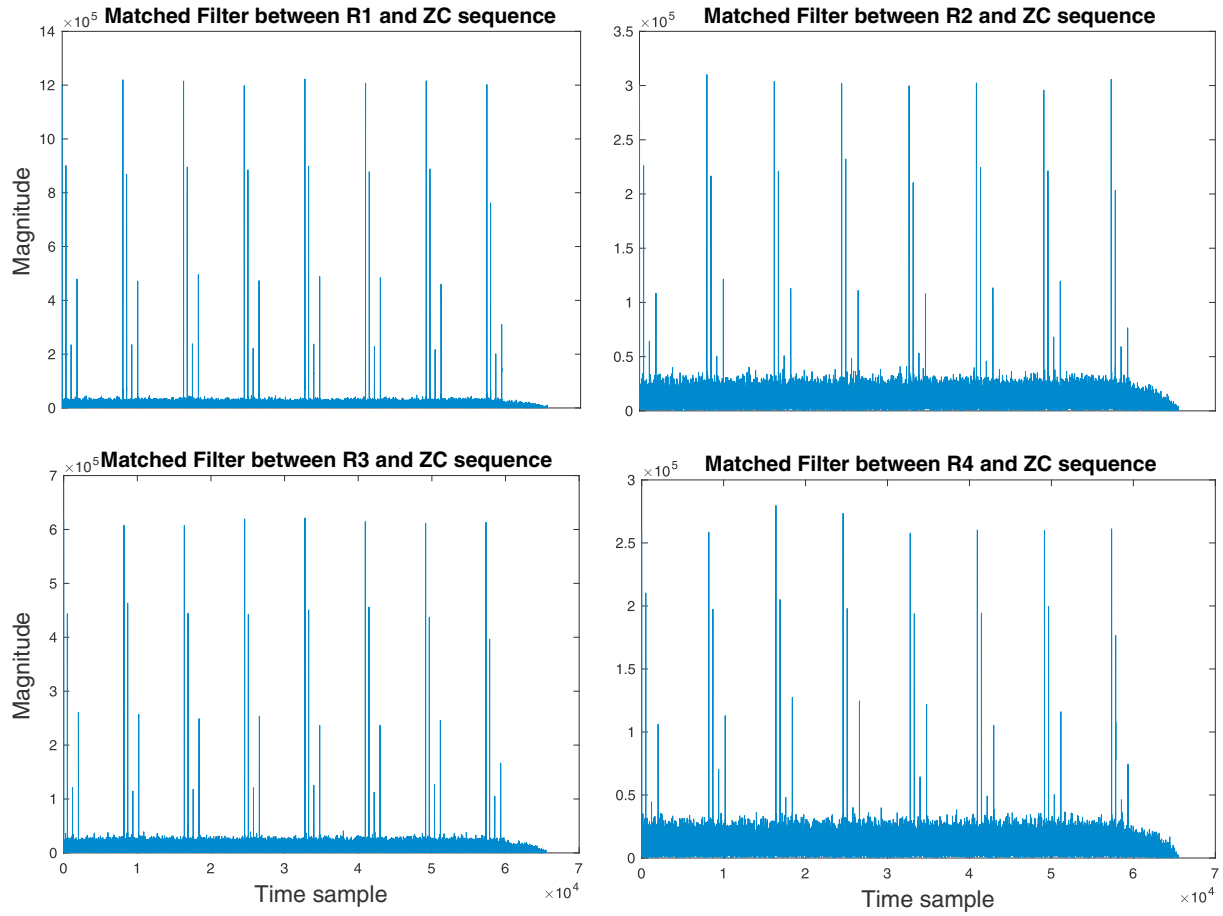

Figure 4. Single snapshot matched filter between each receiver and ZC sequence taken on 24 January 2016 at 00:00:18. Each spike represents the arrival of a length 2^{13} sample ZC signal from a transmitter.

All receivers coherently recorded four snapshots of 2^{16} samples taken at sample rate 1.25 MHz every 15 min. Figure 4 shows matched filter outputs between the transmitted ZC sequence and all receivers for a single snapshot. The matched filter output $\mathbf{m}_i$ of receiver i is defined as

$$\mathbf{m}_i[t] = \sum_{m=-\infty}^{\infty} \mathbf{y}_i[m]\mathbf{z}[t-m], \tag{23}$$

where $\mathbf{y}_i[t]$ represents index t of the measurement vector from receiver i and $\mathbf{z}$ is the unshifted ZC sequence transmitted by T1. Each peak in Figure 4 confirms the arrival of a ZC sequence, the first peak being from T1, the second from T2, and so on. Because the four transmitters each sent repeating 2^{13} sample waveforms, the four arrival spikes in the matched filter are expected to repeat every 2^{13} samples (eight repetitions per snapshot). The magnitude of each spike roughly represents the strength of the path between each transmitter and receiver.

We note that the arrival of the ZC sequence from T3 and T4 in Figure 4 is significantly weaker than the others. We explore two possible explanations, first that both T3 and T4 are positioned at significantly lower elevations than T1 and T2; thus, the horizon presents a greater obstacle. The decreased receive power may be the result of signal attenuation from propagating over the horizon; however, this does not explain why the signal from T4 arrives stronger than that of T3. Second, multipath environments can cause fading (Foschini & Gans, 1998), resulting in null zones where the signal and its reflections effectively cancel each other out. It is possible that the receiver array lies in a null zone for the signals from T3.

6. Results

Receiver noise variance was not recorded during the measurements. We assume that each receiver was subject to the same noise level for the entire testing period; thus, received power represents some scaling of SNR.

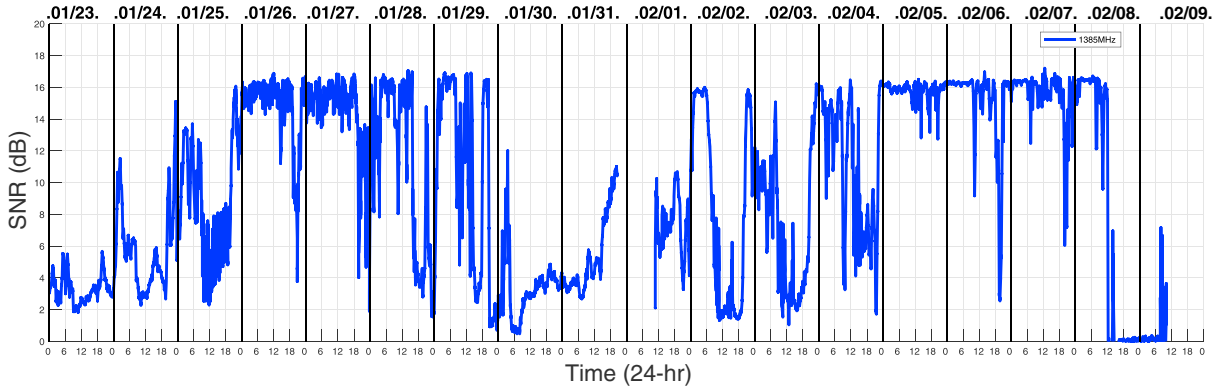

Figure 5. Average received power (dB) over the test period from 23 January to 9 February 2016.

Average received power was calculated as $P_r = \frac{1}{N_R}\|\mathbf{Y}\|_F^2$ for each snapshot $\mathbf{Y} \in \mathbb{C}^{N_R \times 2^{16}}$. The average received power over the full 18 day test period between 23 January and 9 February 2016 is plotted in Figure 5. Note that the array went down for 18 h on 31 January, leading to a short gap in the data.

It is well documented that atmospheric ducts, particularly evaporation ducts, can increase the SNR of over the horizon EM signals (Gerstoft et al., 2003; Haack & Burk, 2001). We assume that periods for which the received power is at a maximum are indicative of some form of ducting (Vasudevan et al., 2007). Using the periods between 25–29 January and 5–8 February as examples of ducting events, we analyze the impact of ducting on the reconstructed path angle pairs of $\hat{\mathbf{H}}^a$ from the experimental data.

All receiver returns were processed using compressive MIMO beamforming. The objective was to visualize the evolution of the multipath channel over time. The data were divided into 2 h intervals, 32 snapshots per interval (4 snapshots per 15 min = 32 snapshots per 2 h), and the estimate $\hat{\mathbf{H}}^a$ from each snapshot was normalized to limit local SNR fluctuations. All normalized estimates of $\hat{\mathbf{H}}^a$ within an interval were averaged to produce

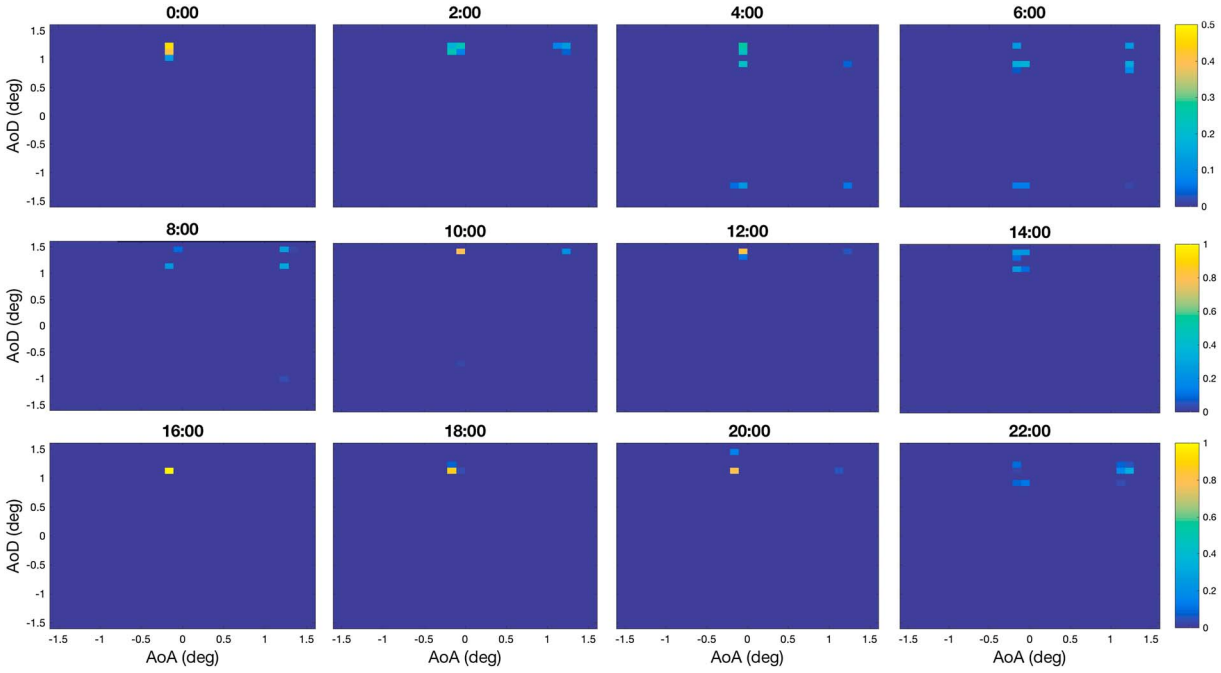

Figure 6. Averaged normalized path gain $\hat{\mathbf{H}}^a_{\text{int}}$ (from equation (24)) over 2 h (32 snapshot) intervals versus AoA and AoD taken on 24 January 2016.

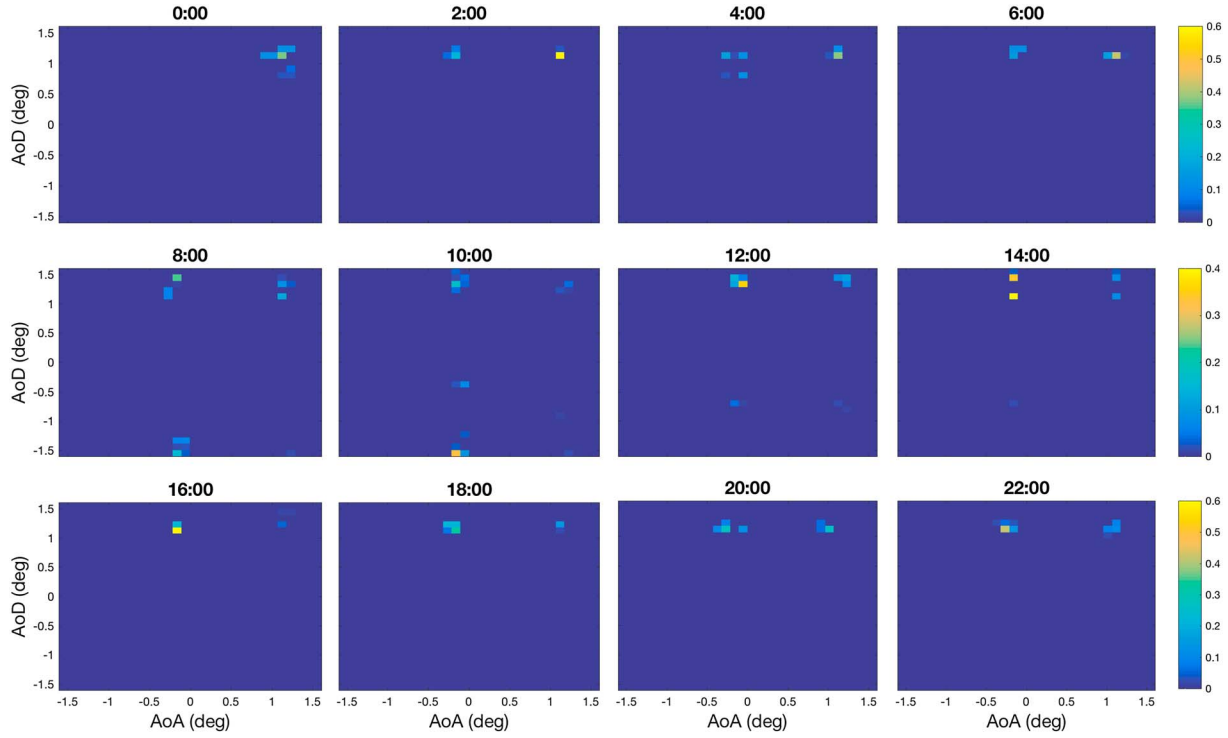

Figure 7. Averaged normalized path gain $\hat{\mathbf{H}}_{\text{int}}^{a}$ (from equation (24)) over 2 h (32 snapshot) intervals versus AoA and AoD taken on 25 January 2016.

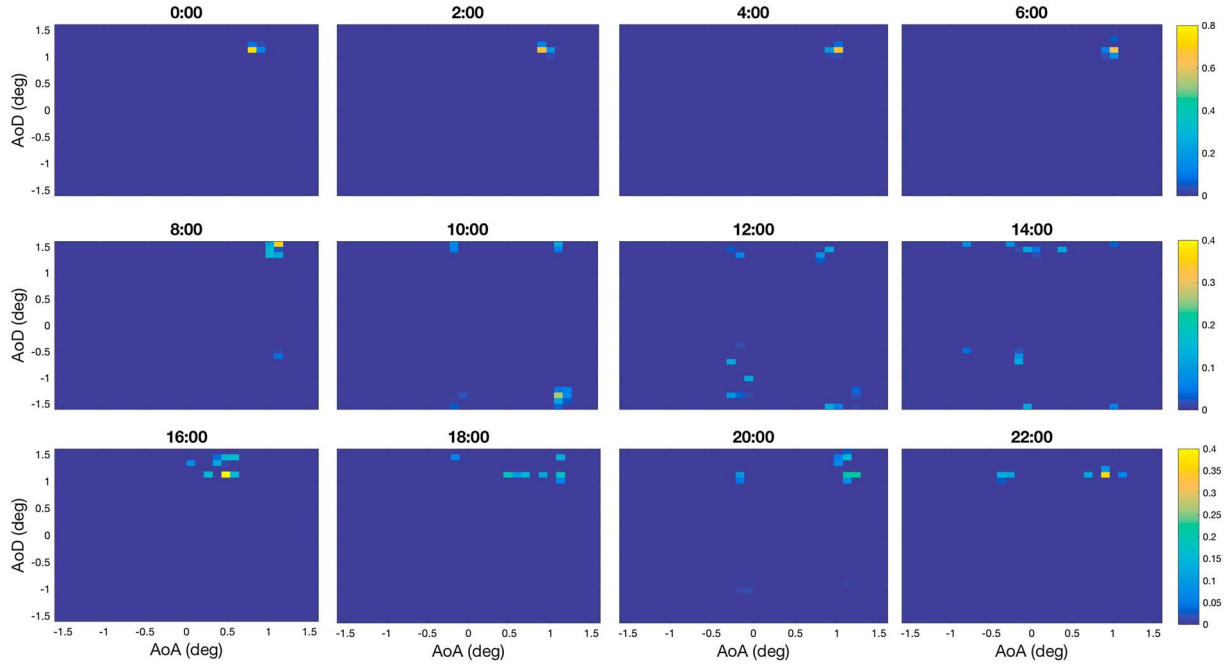

Figure 8. Averaged normalized path gain $\hat{\mathbf{H}}_{\text{int}}^{a}$ (from equation (24)) over 2 h (32 snapshot) intervals versus AoA and AoD taken on 26 January 2016.

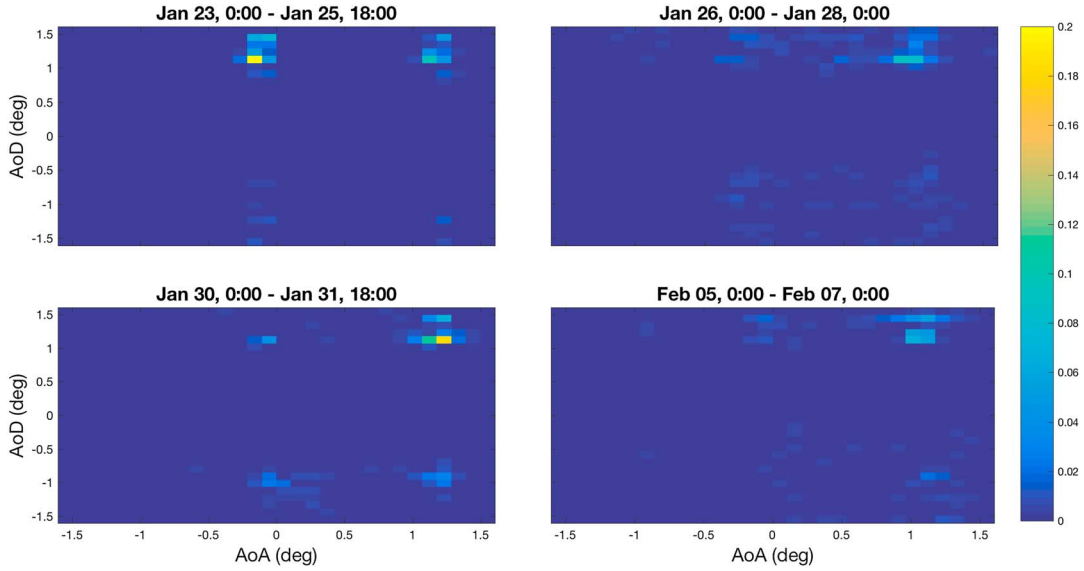

Figure 9. Averaged normalized path gain $\hat{\mathbf{H}}^a_{\text{int}}$ (from equation (24)) over long intervals of high- and low-received power.

$\hat{\mathbf{H}}^a_{\text{int}}$, representing the fraction of path gain through each angle during the interval, normalized to account for power fluctuations between snapshots. Formally,

$$\hat{\mathbf{H}}^a_{\text{int}} = \frac{1}{N}\sum_{n=1}^{N} \frac{\hat{\mathbf{H}}^a_n}{\sum_{i,j} |\hat{\mathbf{H}}^a_{n,i,j}|}, \tag{24}$$

where $\hat{\mathbf{H}}^a_{n,i,j}$ is the (i,j)th element of the estimated angular domain channel matrix from snapshot n and N is the number of snapshots in the interval. Note that the elements of each $\hat{\mathbf{H}}^a_{\text{int}}$ sum to one. $\hat{\mathbf{H}}^a_{\text{int}}$ is plotted in Figures 6–8 for all 2 h intervals between 24 January and 26 January 2016.

We observe from the received power measurements of Figure 5 that an atmospheric duct existed on 26 January. Figures 6–8 show the evolution of the multipath channel from 24 January to 26 January. On 24 January the channel appears stable. There is little fluctuation in received power (mostly occurring between midnight and 6 a.m.), and two dominant path angle pairs are present at each interval. On 25 January, the received power measurements from Figure 5 indicate the possible formation of a weak duct between midnight and 10 a.m. and a strong duct after 6 p.m. Active path angle pairs from 25 January presented in Figure 7 do not show significant variation from those of 24 January. Again, two dominant path angle pairs are present in the majority of the data.

Received power on 26 January (see Figure 5) indicate the presence of a duct. Figure 8 shows that the multipath channel varied rapidly during daylight hours but was stable and indistinguishable from a nonducting channel during nighttime. The impact of ducting appears to be a lack of stability in the active path angle pairs, particularly in daylight hours. Figure 9 shows $\hat{\mathbf{H}}^a_{\text{int}}$ over much longer intervals of low and high measurements of received power. During low-received power measurements active path angle pairs are distributed tightly about specific receive angles, while high-received power measurements lead to more unpredictable path angle pairs. It is possible that during periods of high-received power nonlinearities in the receiver hardware caused inaccuracies in the data and is responsible for the increased variability of active path angle pairs during ducting, but this does not explain why these path angle pairs appear to fluctuate only during daylight hours in Figure 8.

7. Conclusion

Compressive MIMO beamforming was simulated and applied to data recorded from a MIMO system. Simulations showed that compressive MIMO beamforming is capable of accurately identifying multipath signals with higher resolution than conventional beamforming and the 2-D MUSIC algorithm. A MIMO array was set up in a ducting hot spot along the coast of Southern California for the purpose of monitoring the evolution

of its multipath channel over time. Matched filter processing of the received data confirmed the arrival of signals from the transmitters. An optimal estimate of the channel was made 4 times every 15 min. From each channel measurement an angular domain channel matrix was calculated using compressive MIMO beamforming. The evolution of active path angle pairs from the angular domain channel matrix was examined over the measurement period.

The received power from the channel was used to determine the presence of ducting with periods of high-received power assumed to indicate ducting and low-received power to indicate a standard atmosphere. Two ducting events lasting multiple days were observed over the measurement period. The MIMO paths did not appear strongly related to received power or predictive of ducting. The active path angle pairs observed during ducting events were found to come from a wider range of path angles. Path angle pairs traveled by communications signals during ducting events were found to sometimes change quickly and unpredictably compared to those observed when no ducts were present.

No conclusive evidence was found that active path angle abnormalities from received MIMO communications signals can be used to predict ducting. The data, however, are only representative of one nearshore channel between points in Southern California, and results may differ for channels in alternate locations. More data collection is required before conclusions can be drawn about the relation between ducting and the shape of a MIMO multipath channel. We suggest that refractivity profiles be taken alongside MIMO data in future-related work so that the precise shape of the duct can be compared with the active path angle pairs of the MIMO signal.

Appendix A

A1. The 2-D Conventional Beamforming

Like compressive MIMO beamforming, conventional beamforming (CBF) takes in a channel estimate $\hat{\mathbf{H}}$ and outputs an estimate of the angular domain channel matrix $\mathbf{H}^a_{\text{CBF}}$. From (2), a channel matrix $\mathbf{H}$ is the sum of P rank 1 matrices, each representing a path from transmitter to receiver. With this understanding we define dictionaries (Tse & Viswanath, 2005)

$$\mathbf{S}_R \in \mathbb{C}^{N_R \times Q_R} = \left[\mathbf{a}_R(-\theta_{\min}), \ldots, \mathbf{a}_R(\theta_{\max})\right], \tag{A1}$$

$$\mathbf{S}_T \in \mathbb{C}^{N_T \times Q_T} = \left[\mathbf{a}_T(-\phi_{\min}), \ldots, \mathbf{a}_T(\phi_{\max})\right], \tag{A2}$$

where Q_R and Q_T are the number of bins into which the transmit and receive angle space is divided. The dictionaries in (A1) and (A2) have columns representing the array responses from signals arriving and departing from different angles. Larger Q_R and Q_T result in dictionaries that more finely divide the angular spectrum.

The angular domain representation of a channel $\mathbf{H}$ for conventional beamforming (Tse & Viswanath, 2005) is defined as

$$\mathbf{H}^a_{\text{CBF}} = \mathbf{S}_R^H \mathbf{H} \mathbf{S}_T. \tag{A3}$$

Unlike compressive MIMO beamforming, the formulation of $\mathbf{H}^a_{\text{CBF}}$ in equation (A3) does not assume sparsity in $\mathbf{H}^a_{\text{CBF}}$, so the CBF estimate of $\mathbf{H}^a$ is inherently different from that of compressive MIMO beamforming.

A2. The 2-D MUSIC

The 2-D MUSIC algorithm (Zhang et al., 2010) is a variation of the popular MUSIC subspace method (Schmidt, 1986). Increased resolution is achieved by separating the signal and noise subspaces of the channel matrix through eigen decomposition. The idea is that contributions to the channel $\mathbf{H}$ from noise are contained in the smallest eigenvalues of the channel covariance matrix, and by removing such eigenvalues, a denoised version of the channel is created.

The channel covariance is

$$\mathbf{R} = E[\mathbf{h}\mathbf{h}^H], \tag{A4}$$

where $\mathbf{h} = \text{vec}(\mathbf{H})$, which has eigen decompsition

$$\mathbf{R} = \mathbf{U}_S \mathbf{\Lambda}_S \mathbf{U}_S^H + \mathbf{U}_N \mathbf{\Lambda}_N \mathbf{U}_N^H. \tag{A5}$$

Here $\mathbf{U}_S$ and $\mathbf{U}_N$ are the matrices whose columns contain the eigenvectors of the signal and noise subspaces, and $\mathbf{\Lambda}_S$, $\mathbf{\Lambda}_N$ are diagonal matrices whose elements are the corresponding eigenvalues. If the signal primarily travels through n paths, the dimension of the signal subspace is n. Under this assumption $\mathbf{U}_S$ will contain the n eigenvectors corresponding to the n largest eigenvalues. The spectrum function for 2-D MUSIC is given as (Wang, 2012)

$$F(\theta,\phi)=\frac{1}{\tilde{\mathbf{a}}^H(\theta,\phi)\mathbf{U}_N\mathbf{U}_N^H\tilde{\mathbf{a}}(\theta,\phi)}. \tag{A6}$$

$F(\theta,\phi)$ is a continuous function which represents the relative strength of the signal traveling through angles (θ,ϕ), similar to estimates of $\mathbf{H}^a$ from CBF and compressive MIMO beamforming. An example of $F(\theta,\phi)$ is shown in Figure 2.

Acknowledgments
This paper was sponsored by funding from the Office of Naval Research (ONR) grant [10.13039/100000006] (N00014-15-1-2490). The authors extend special thanks to Silvus Technologies for setting up and collecting data from the MIMO test bed. Data set can be accessed at https://doi.org/10.6084/m9.figshare.5035178.v2.

References

Bartlett, M. S. (1948). Smoothing periodograms from time series with continuous spectra. *Nature*, *161*(4096), 686–687.
Bickel, P. J., Ritov, Y. A., & Tsybakov, A. B. (2009). Simultaneous analysis of Lasso and Dantzig selector. *The Annals of Statistics*, *37*(4), 1705–1732.
Biguesh, M., & Gershman, A. B. (2006). Training-based MIMO channel estimation: A study of estimator tradeoffs and optimal training signals. *IEEE Transactions on Signal Processing*, *54*(3), 884–893.
Bolcskei, H., Gesbert, D., & Paulraj, A. J. (2002). On the capacity of OFDM-based spatial multiplexing systems. *IEEE Transactions on Communications*, *50*(2), 225–234.
Candes, E., & Tao, T. (2007). The Dantzig selector: Statistical estimation when P is much larger than N. *The Annals of Statistics*, *35*, 2313–2351.
Candes, E. J. (2008). The restricted isometry property and its implications for compressed sensing. *Comptes Rendus Mathematique*, *346*(9–10), 589–592.
Chan, P. W., Lee, D. C., Tam, F. K., Chih-Lin, I., Cheng, R. S., & Lau, V. K. (2008). Angular-domain channel model and channel estimation for MIMO system. In *IEEE global telecommunications conference* (pp. 1–5). New Orleans, LA: GLOBECOM.
Chen, S. S., Donoho, D. L., & Saunders, M. A. (2001). Atomic decomposition by basis pursuit. *SIAM Review*, *43*(1), 129–159.
Chu, D. (1972). Polyphase codes with good periodic correlation properties (corresp.) *IEEE Transaction on Information Theory*, *18*(4), 531–532.
Craig, K. H., & Levy, M. F. (1991). Parabolic equation modeling of the effects of multipath and ducting on radar systems. *IEEE Proceedings F*, *138*(2), 153–162.
Daubechies, I., Defrise, M., & De Mol, C. (2004). An iterative thresholding algorithm for linear inverse problems with a sparsity constraint. *Communications on Pure and Appled Mathematics*, *57*(11), 1413–1457.
Donoho, D. L. (2006). Compressed sensing. *IEEE Transactions on Information Theory*, *52*(4), 1289–1306.
Foschini, G. J., & Gans, M. J. (1998). On limits of wireless communications in a fading environment when using multiple antennas. *Wireless Personal Communications*, *6*(3), 311–335.
Gerstoft, P., Rogers, L. T., Hodgkiss, W. S., & Wagner, L. J. (2003). Refractivity estimation using multiple elevation angles. *IEEE Journal of Oceanic Engineering*, *28*(3), 513–525.
Gerstoft, P., Xenaki, A., & Mecklenbräuker, C. F. (2015). Multiple and single snapshot compressive beamforming. *The Journal of the Acoustical Society of America*, *138*(4), 2003–2014.
Haack, T., & Burk, S. D. (2001). Summertime marine refractivity conditions along coastal California. *Journal of Applied Meteorology*, *40*(4), 673–687.
Mallat, S. G., & Zhang, Z. (1993). Matching pursuits with time-frequency dictionaries. *IEEE Transactions on Signal Processing*, *41*(12), 3397–3415.
Mecklenbrauker, C. F., Gerstoft, P., & Zochmann, E. (2017). C-LASSO and its dual for sparse signal estimation from array data. *Signal Processing*, *130*(18), 204–216.
Pesavento, M., Mecklenbrauker, C. F., & Bohme, J. F. (2004). Multidimensional rank reduction estimator for parametric MIMO channel models. EURASIP. *Journal on Applied Signal Processing*, *2004*(9), 1354–1363.
Rudelson, M., & Vershynin, R. (2008). On sparse reconstruction from Fourier and Gaussian measurements. *Communications on Pure and Appled Mathematics*, *61*(8), 1025–1045.
Schmidt, R. (1986). Multiple emitter location and signal parameter estimation. *IEEE Transactions on Antennas and Propagation*, *34*(3), 276–280.
Steffens, C., Yang, Y., & Pesavento, M. (2016). Multidimensional sparse recovery for MIMO channel parameter estimation. In *Proceedings of the 24th IEEE European Signal Processing Conference (EUSIPCO)*. Budapest, Hungary: EUSIPCO.
Tibshirani, R. (1996). Regression shrinkage and selection via the LASSO. *Journal of the Royal Statistical Society. Series B (Methodological)*, *58*(1), 267–288.
Timmins, I. J., & O'Young, S. (2009). Marine communications channel modeling using the finite-difference time domain method. *IEEE Transactions on Vehicular Technology*, *58*(6), 2626–2637.
Tipping, M. E. (2001). Sparse Bayesian learning and the relevance vector machine. *Journal of Machine Learning Research*, *6*(2001), 211–244.
Tse, D., & Viswanath, P. (2005). *Fundamentals of wireless communication*. New York: Cambridge University Press.
Vasudevan, S., Anderson, R. H., Kraut, S., Gerstoft, P., Rogers, L. T., & Krolik, L. J. (2007). Recursive Bayesian electromagnetic refractivity estimation from radar sea clutter. *Radio Science*, *42*, RS2014. https://doi.org/10.1029/2005RS003423
Wagner, M., Gerstoft, P., & Rogers, T. (2016). Estimating refractivity from propagation loss in turbulent media. *Radio Science*, *51*, 1876–1894. https://doi.org/10.1002/2016RS006061
Wang, H. M., Gao, X. Q., Jiang, B., You, X. H., & Hong, W. (2007). Efficient MIMO channel estimation using complementary sequences. *IET Communications*, *5*, 962–969.
Wang, W. Q. (2012). Virtual antenna array analysis for MIMO synthetic aperture radars. *International Journal of Antennas and Propagation*, *2012*(1), 587–596.
Zhang, X., Xu, L., & Xu, D. (2010). Direction of departure (DOD) and direction of arrival (DOA) estimation in MIMO radar with reduced-dimension MUSIC. *IEEE Communication Letters*, *14*(12), 1161–1163.